Occurrence of pristine aerosol environments on a polluted planet

Douglas S. Hamilton[1], Lindsay A. Lee, Kirsty J. Pringle, Carly L. Reddington, Dominick V. Spracklen, and Kenneth S. Carslaw

School of Earth and Environment, University of Leeds, Leeds LS2 9JT, UK

Edited by John H. Seinfeld, California Institute of Technology, Pasadena, CA, and approved November 13, 2014 (received for review August 11, 2014)

Natural aerosols define a preindustrial baseline state from which the magnitude of anthropogenic aerosol effects on climate are calculated and are a major component of the large uncertainty in anthropogenic aerosol–cloud radiative forcing. This uncertainty would be reduced if aerosol environments unperturbed by air pollution could be studied in the present-day atmosphere, but the pervasiveness of air pollution makes identification of unperturbed regions difficult. Here, we use global model simulations to define unperturbed aerosol regions in terms of two measures that compare 1750 and 2000 conditions—the number of days with similar aerosol concentrations and the similarity of the aerosol response to perturbations in model processes and emissions. The analysis shows that the aerosol system in many present-day environments looks and behaves like it did in the preindustrial era. On a global annual mean, unperturbed aerosol regions cover 12% of the Earth (16% of the ocean surface and 2% of the land surface). There is a strong seasonal variation in unperturbed regions of between 4% in August and 27% in January, with the most persistent conditions occurring over the equatorial Pacific. About 90% of unperturbed regions occur in the Southern Hemisphere, but in the Northern Hemisphere, unperturbed conditions are transient and spatially patchy. In cloudy regions with a radiative forcing relative to 1750, model results suggest that unperturbed aerosol conditions could still occur on a small number of days per month. However, these environments are mostly in the Southern Hemisphere, potentially limiting the usefulness in reducing Northern Hemisphere forcing uncertainty.

natural aerosol | pristine regions | radiative forcing | preindustrial | baseline

Natural aerosol and precursor gas emissions are an important part of the climate system (1, 2). Improved understanding of how natural emissions determine aerosol concentrations in different environments is important for reducing the uncertainty in model estimates of cloud radiative forcing over the industrial period (3, 4). Even under the assumption that natural emissions do not change with time, the magnitude of preindustrial (PI) to present-day (PD) aerosol–cloud forcing is very sensitive to natural emissions and processes in the PI because of the nonlinear relationship between aerosol concentrations, cloud drop concentrations, and cloud albedo (3–7). Other more complex cloud adjustments are also likely to respond sensitively to small changes in aerosol under clean conditions (6, 8). Improved understanding of the PI "baseline aerosol" is necessary to reduce the uncertainty in aerosol–cloud forcing estimates, hence the total anthropogenic radiative forcing and thereby also the climate sensitivity which depends on it (4, 9). Natural emissions may also change in the future due to climate change (1), causing a natural aerosol radiative feedback on climate (10). To reduce these large climate model uncertainties, it is important to know where on Earth we can study aerosols in environments that most closely resemble a natural, unperturbed state (4, 11).

It has been argued that regions in which aerosols are unperturbed by air pollution no longer exist in today's atmosphere (12). If this were so, then much of the uncertainty in indirect forcing may be irreducible (4). Even in regions dominated by natural emissions of sea spray, volcanic sulfates, marine dimethyl sulphide, or terrestrial biogenic volatile organic compounds, the aerosol state can still be strongly perturbed by long-range transport from anthropogenic sources (e.g., refs. 10–13). Studies of natural emissions and processes have typically focused on remote regions such as the high northern latitude boreal forest (14), the Brazilian rainforest (15, 16), and the Southern Ocean (17). However, the choice of location tends to be based on the physical remoteness of the site and the strength of local natural emissions, but with little consideration of how closely the aerosol state truly resembles unperturbed conditions.

Several definitions of pristine, natural or "clean background" aerosol environments have been used when analyzing observations, including particle number concentrations (18), the concentration of a particular species such as carbon monoxide or particulate black carbon (19), the location (14, 16), or a combination of factors (6). However, operational definitions suffer from not knowing how much the environment is influenced by a pervasive background of anthropogenic aerosol, which is unlikely to be detectable in observations. It is also not always possible to define pristine environments in terms of the lowest observed aerosol concentration at a particular site because often such conditions are associated with strong scavenging by precipitation and will not represent and behave like the true climatological state in the PI. Remote oceans can provide an insight into how clouds respond to changes in aerosol starting from a very low aerosol baseline (6), but are unlikely to be good analogs for aerosol in all PI regions, which will often have been strongly affected by emissions from natural forest fires (20), volcanic activity (3), or terrestrial biogenic emissions (21). There is therefore no single globally applicable aerosol state that defines the preindustrial atmosphere. Rather, the state changes spatially and

Significance

Uncertainty in aerosol forcing of climate since the preindustrial era hampers efforts to quantify the sensitivity of global temperature to radiative perturbations caused by human activity. Because forcings are referenced to preindustrial conditions, a large part of the uncertainty will be reduced only by accurately defining pristine aerosol conditions before air pollution. We show that pristine conditions should still be observable on a few days per month in many regions of the Earth. However, pristine cloudy regions, which are of most importance for forcing uncertainty, occur almost entirely in the Southern Hemisphere. Reduction in uncertainty of predominantly Northern Hemisphere forcing may therefore have to rely on measurements from a different hemisphere, which will limit the extent to which uncertainties can be reduced.

Author contributions: D.S.H., D.V.S., and K.S.C. designed research; D.S.H., L.A.L., K.J.P., and C.L.R. performed research; D.S.H., L.A.L., C.L.R., D.V.S., and K.S.C. analyzed data; and D.S.H., D.V.S., and K.S.C. wrote the paper.

The authors declare no conflict of interest.

This article is a PNAS Direct Submission.

[1]To whom correspondence should be addressed. Email: d.hamilton@leeds.ac.uk.

This article contains supporting information online at www.pnas.org/lookup/suppl/doi:10.1073/pnas.1415440111/-/DCSupplemental.

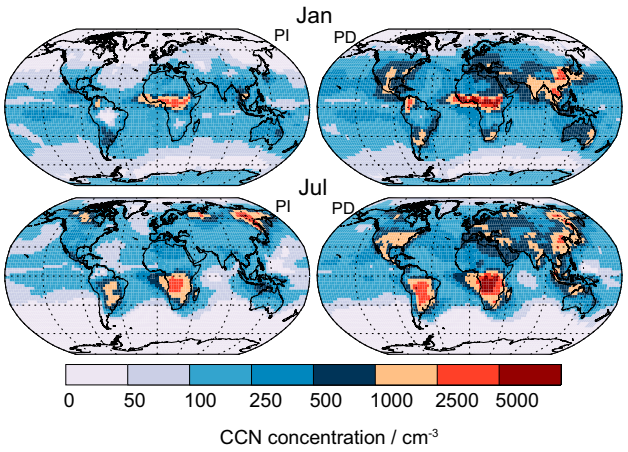

Fig. 1. PI (1750) and PD (2000) monthly mean CCN concentrations in January and July. CCN concentrations are defined as the aerosol concentration with a dry diameter above 50 nm and calculated at cloud base (~915 hPa).

seasonally. Global models provide an alternative, and perhaps the only, way of estimating the properties and behavior of aerosols in a preindustrial reference state, and can at least point to where a pristine aerosol state is likely to be observable today.

The purpose of this paper is to define regions of the Earth where PD aerosol (year 2000) looks and behaves most like it did in a PI reference state (year 1750). We use the term pristine to refer to such regions, meaning aerosol in an original (i.e., preindustrial) state, although the term can often be used misleadingly to imply extremely low aerosol concentrations. Anthropogenic emissions in 1750 were not zero (22), and our reference year is therefore not truly "prehuman" (12), but is appropriate for defining the properties and behavior of aerosols in a reference state that is used for radiative forcing calculations (23). We focus our analysis on cloud condensation nuclei (CCN) because of the high sensitivity of cloud radiative forcing to the aerosol load (24).

Based on the results of a global aerosol microphysics model (3, 4, 25), we use two measures of similarity of aerosol between the PI and PD. First, we compare the aerosol states: On how many days are PD CCN concentrations similar to those in the PI? Air pollution tends to be episodic in remote regions, so it is not appropriate to compare longer time averages because a few polluted days will make the whole period appear mildly polluted. Secondly, we compare the aerosol response: How similar is the CCN response (or sensitivity) to perturbations in emissions and processes in the PI and PD? The similarity of aerosol responses is an essential additional factor in defining pristine regions, which cannot be addressed using observations alone. It is conceivable that two periods in the aerosol historical record could have similar CCN concentrations (the aerosol state) but respond differently to perturbations because those two states were generated through a different series of emissions and/or processes. By comparing the responses in the PI and PD, we can identify regions where the PD aerosol is "behaving" like it did in the PI.

To test the similarity of aerosol states, we quantify changes in CCN concentration between 1750 and 2000. To test the similarity of aerosol responses in 1750 and 2000, we compare the sensitivity of CCN to 28 model parameters representing natural and anthropogenic aerosol emissions, microphysical processes, and model structures, with the parameter ranges based on expert elicitation (4, 26). To ensure that the statistics of PI–PD similarity reflect only the change in emissions and associated aerosol processes, we used the same (year 2008) global 3D meteorological reanalyses in 1750 and 2000, which eliminates meteorology as a source of variability between the two years.

Results and Discussion

Properties of the Preindustrial Aerosol. Fig. 1 shows CCN concentrations simulated using the median setting of the model parameters (Table S1) for PI and PD conditions in January and July (a full year of PI CCN concentrations is shown in Fig. S1). We define CCN concentrations as the number concentration of soluble particles with a dry diameter equal to or greater than 50 nm at 915 hPa, approximately cloud base for stratiform low-level clouds. Contrary to previous suggestions (12), our model results suggest that a significant land–ocean contrast in CCN concentrations could also have existed in the PI. Averaged over a year, the mean PI CCN concentrations over Northern Hemisphere (NH) land regions are 36% higher than the Southern Hemisphere (SH) land regions (NH = 186 cm^{-3} and SH = 137 cm^{-3}), while, over ocean regions, they are almost identical (NH = 61 cm^{-3} and SH = 64 cm^{-3}). Fires are an important source of high PI CCN concentrations, particularly in Africa, South America, and northern boreal regions in summer. The PI land–ocean contrast in CCN concentrations is particularly large in July, lying between 0 cm^{-3} and 100 cm^{-3} over most extratropical ocean regions and 100 cm^{-3} and 500 cm^{-3} over the majority of the land, with peak CCN concentrations greater than 2,500 cm^{-3} in African savannah burning regions and greater than 5,000 cm^{-3} in Siberian boreal regions. Another factor affecting the PI land–ocean contrast is the higher abundance of biogenic organic compounds over land, which causes the growth of small nucleated particles to CCN sizes (27). The model we use here does not account for the role of organic compounds in the first stages of nucleation itself, which would further increase the land–ocean contrast (21).

Histograms (Fig. 2) of PI and PD CCN concentrations (based on Fig. 1 and Fig. S1) show that although the occurrence of high CCN concentrations is similar in the PI and PD, the most frequent oceanic CCN concentrations are centered around 80 cm^{-3} compared with about 180 cm^{-3} over land. The PD histograms show a much greater influence of pollution over land compared with oceanic regions, with the most frequent CCN concentration remaining around 80 cm^{-3} over the ocean, but increasing to more than 500 cm^{-3} over land. Despite the differences between PI and PD aerosol concentrations, there is considerable overlap

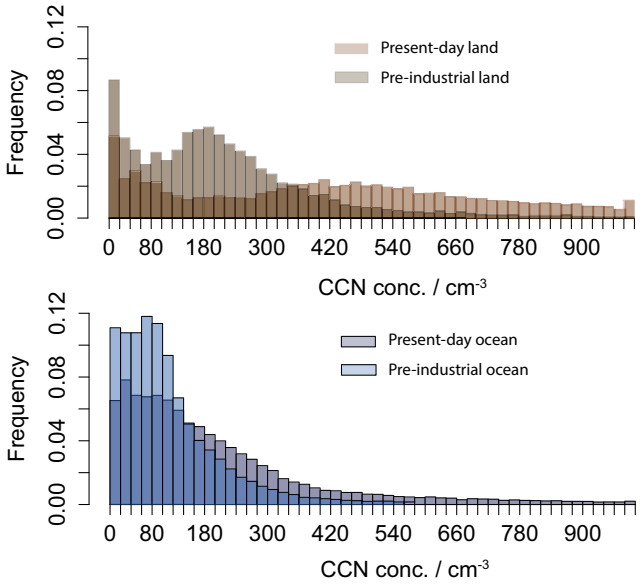

Fig. 2. PI and PD global modeled annual mean CCN concentrations over land and ocean grid cells, calculated from daily mean CCN concentrations at cloud base (~915 hPa). The third color indicates overlap of the two distributions. The maximum CCN bin concentration is set to 1,000 cm^{-3}, although a small fraction exists at higher concentrations.

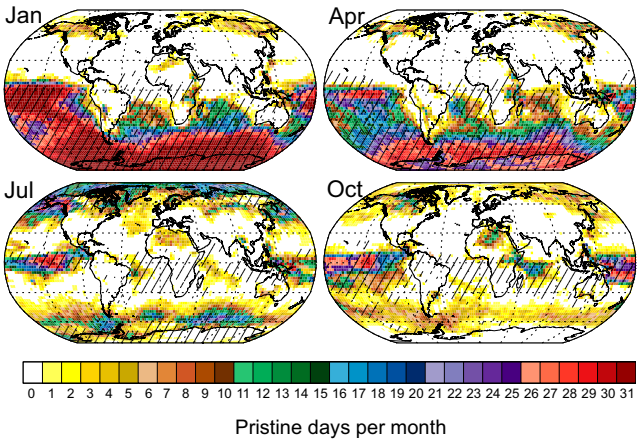

Fig. 3. The occurrence of pristine days in January, April, July, and October, based on two definitions. Colors show the number of days per month on which PI and PD CCN concentrations differ by no more than ±20% in that grid cell at cloud base (~915 hPa). Stippling shows regions where the sensitivities of PI and PD CCN to 28 model parameters are similar ($r^2 \geq 0.9$) in that grid cell at cloud base. Pristine regions are those that exhibit both a similar PI and PD CCN concentration and a similar PI and PD response to the 28 parameters.

of the CCN histograms, particularly over oceans at low CCN concentrations, suggesting that regions exist today that could be analogs for PI environments.

The estimated uncertainty (SD) in PI CCN concentrations varies spatially and temporally (Fig. S2). The parametric uncertainty was calculated by performing a Monte Carlo sampling of validated Bayesian emulators conditioned on an ensemble of 168 model simulations covering the joint parameter space of the 28 model parameters (see *SI Methods*). This approach generates a probability density distribution of CCN concentrations caused by the uncertainty in the model input parameters, including their interactions (26). By sampling the model uncertainties, we are able to estimate a plausible range of CCN concentrations in the PI under the assumption that the sources of uncertainty are the same as in the PD (Table S1). Over marine regions, modeled uncertainty in CCN concentrations is typically 20–40% (SD divided by the mean, shown in Fig. S3) between ±60° latitude, up to about 70–90% at higher latitudes and over 100% near the Antarctic continent and very high latitude Arctic regions. In some continental regions, uncertainties exceed 100% of the mean in regions dominated by fires. To further assess how structural uncertainties potentially alter the pristine regions presented in this study, future studies using a range of models would need to be undertaken.

The Occurrence of Pristine Days. Fig. 3 shows the similarity of CCN concentrations in the PI and PD in terms of the number days that concentrations are within ±20% (a full year is shown in Fig. S4). The threshold of ±20% in concentration is based on the estimated CCN measurement uncertainty across the majority of datasets compiled by Spracklen et al. (28), and Fig. S5 shows the daily fraction of the Earth defined as pristine when this threshold is set to values ranging between ±0% and ±100%.

The occurrence of pristine CCN regions in the PD atmosphere is highly variable in space and time, with the frequency of pristine days lying between 0% and 100% in a given month. Averaged over a full year, approximately one third (Table 1) of the SH has CCN concentrations similar to the PI, with a maximum spatial coverage over SH ocean regions in the SH summer when every day of the month approaches pristine conditions. In contrast, less than 9% of the NH is pristine, with a maximum coverage of about 15%, also in the summer. In many major shipping regions [e.g., Capaldo et al. (29)], anthropogenic perturbations to aerosol concentrations are large enough that the region is classed as nonpristine. The equatorial Pacific Ocean is the most persistently pristine environment, most likely due to the dominant local marine emission source and effective barrier to NH interhemispheric transport of anthropogenic pollution provided by the intertropical convergence zone. In agreement with observational (19) and modeling studies (11), we identify the southern Pacific Ocean (approximately 20°S–60°S, 90°W –180°W) as a large region close to pristine, especially during SH summer when monthly mean PD CCN concentrations in this region are in the range of 53–285 cm^{-3} (median 104 cm^{-3}), when the main natural source of CCN is from DMS-derived sulfate aerosol (30). A Southern Ocean summertime band of pristine CCN exists between 50°S and 65°S, with generally low monthly mean PD CCN concentrations of 20–153 cm^{-3} (median 58 cm^{-3}), when natural emissions of sea spray are the dominant aerosol source (17). The midlatitude Pacific and Atlantic Oceans deviate from a pristine state for more of the year than at higher and lower latitudes, mainly due to assumed increases in emissions from South American and African tropical fire regions (31) which is assumed to be due to increased anthropogenic activity. Generally, SH continental land masses have sparse regions of pristine CCN concentrations.

In the NH, prolonged pristine periods generally occur only over continental regions above 60°N, such as in boreal Canada (32) and Russia (33), where aerosol is affected strongly by natural forest fire emissions. Here, CCN concentrations are highly variable, but generally range from 100 to 1,000 cm^{-3}. The high Arctic (75°N and above) is frequently pristine during the NH summer, with low monthly mean CCN concentrations in July of 39–142 cm^{-3} (median 55 cm^{-3}), but strongly and persistently polluted during winter and spring, consistent with the seasonal cycle of Arctic haze controlled by scavenging processes (34, 35). There are almost no marine pristine days during NH winter and spring, and very few regions are persistently pristine over a month. In NH midlatitude regions, there are no pristine days at any time of the year. In particular, the North Pacific Ocean is impacted by transport of pollution from East Asia to North America (36) and is a region where we find no pristine days in the main transport periods.

Our confidence in the extent and location of pristine regions depends on the modeled CCN uncertainty as well as the assumed tolerance used to compare PI and PD CCN (set at ±20%, as above). Fig. S6 shows the effect of changing the tolerance to 10%, 30%, and 50%. This range of tolerances is comparable to the modeled relative CCN uncertainty, which is ~20–50% in the main pristine regions (Fig. S3). We have most confidence in regions with a low relative modeled CCN uncertainty (Fig. S3) and a high number of pristine days. The optimum pristine region by this definition is the central Pacific. Although relative uncertainties can be fairly high in other pristine regions, we expect the model uncertainties to be correlated in the PI and PD, giving us more confidence in the model results than indicated by Fig. S3. While meteorological variability is likely to cause interannual variability in the precise location of pristine regions, the principal

Table 1. Fraction of the Earth defined as pristine

	Pristine Fraction				
Month	Global	Ocean	Land	NH	SH
Jan	0.27 (0.32)	0.34 (0.40)	0.09 (0.13)	0.02 (0.06)	0.53 (0.59)
Apr	0.18 (0.25)	0.21 (0.30)	0.08 (0.12)	0.00 (0.03)	0.35 (0.46)
Jul	0.05 (0.14)	0.06 (0.16)	0.02 (0.08)	0.06 (0.15)	0.04 (0.13)
Oct	0.05 (0.11)	0.07 (0.14)	0.01 (0.05)	0.03 (0.09)	0.07 (0.13)
Annual	0.12 (0.21)	0.16 (0.26)	0.02 (0.10)	0.02 (0.08)	0.22 (0.34)

Pristine defined as PI to PD CCN concentration ±20% and similar PI to PD CCN response to 28 parameters covering natural and anthropogenic emissions, processes and model structures. Values in parentheses show the fraction when the concentration change only is considered.

pristine regions (the remote Pacific, Southern Ocean, Arctic, etc.) will be more climatologically persistent features.

The distribution of pristine days is similar at ~2.5 km above sea level (a.s.l.) (Fig. S7), while at ~5 km a.s.l., long-range transport of anthropogenic emissions cause changes in the spatial distributions of SH pristine regions (Fig. S8). However, these free tropospheric aerosols do not affect cloud-base CCN concentrations in the boundary layer, and if they are mixed down to lower altitudes, then they will be included already in our analyzed fields at ~850 m a.s.l.

Changes in CCN Sensitivity Between 1750 and 2000. Stippling in Fig. 3 shows regions where the aerosol sensitivity to perturbations of 28 model parameters covering emissions, microphysical processes and model structures (26) is similar in 1750 and 2000. The parameter sensitivities in each grid cell at cloud base (915 hPa) were calculated by variance decomposition of the CCN distributions that were used to generate the uncertainty in CCN concentrations (Fig. S2). The fractional contribution to variance of each parameter is termed the main effect index (26, 37). We correlated the main effect indices for the 28 parameter perturbations in each grid cell (see the *SI Methods* for a full description) and define regions to be pristine, somewhat arbitrarily, if the coefficient of correlation is greater than 0.9. Fig. 4 shows these correlations at four representative sites.

In regions where CCN concentrations exhibit about 20 or more pristine days in a month, the CCN response to model parameters is generally also similar in both periods. For regions with about 10–19 d of pristine CCN concentration, there is partial overlap with regions with similar CCN sensitivity, while for regions of with less than 10 d per month of pristine CCN concentrations, CCN sensitivities are now different than the PI.

The equatorial Pacific is the largest region that is closest to pristine all year round in terms of the similarity of the aerosol state and the aerosol sensitivity, while other regions vary seasonally between being pristine and not. Other regions with a high number (20 or more) of pristine days and similar CCN sensitivity in one or more months include parts of Alaska and Yukon, the Southern Ocean, Melanesia, southwest Greenland, and the southern Indian Ocean.

Fig. 4 shows the change in PI to PD CCN sensitivity at four grid cells representing four different sites. Melanesia (Fig. 4*A*) has a very similar CCN sensitivity and state in 1750 and 2000, where 99% of January/April/July/October modeled days have PD CCN concentrations within ±20% of PI concentrations. Prevailing winds in this region originate over the Pacific Ocean, bringing clean background air masses and natural marine aerosol (38). Fig. 4*A* shows that both 1750 and 2000 CCN sensitivities are dominated by the same parameters relating to natural emissions and aerosol microphysical processes [volcanic SO_2 and biogenic secondary organic aerosol (SOA) as well as model uncertainties in the Aitken mode width, boundary layer nucleation rates, CCN activation diameter, and the pH of cloud droplets]. In all months, the fraction of variance attributable to anthropogenic emissions is less than about 1%. CCN concentrations and behavior in this location are therefore clearly driven by natural processes.

The eastern Atlantic (Fig. 4*B*) has a different CCN response and state in the two periods. It is located in a region of high aerosol–cloud radiative forcing (4). Many of the main effect indices have changed over the industrial period, indicating an anthropogenic influence on the behavior of the aerosol. In particular, anthropogenic SO_2 emissions and production of SOA from anthropogenic compounds contribute more to CCN variance in the PD than in the PI, and natural emissions of DMS and biomass burning contribute less. This reduction in sensitivity to natural emissions will suppress natural aerosol–climate feedbacks (39).

The Brazilian rainforest (Fig. 4*C*) has a similar CCN response but dissimilar state in the two periods. Although the aerosol state is strongly anthropogenically perturbed by increased biomass burning emissions, these emissions dominate the aerosol sensitivity in both the PI and PD (Fig. 4*C*). While our model results

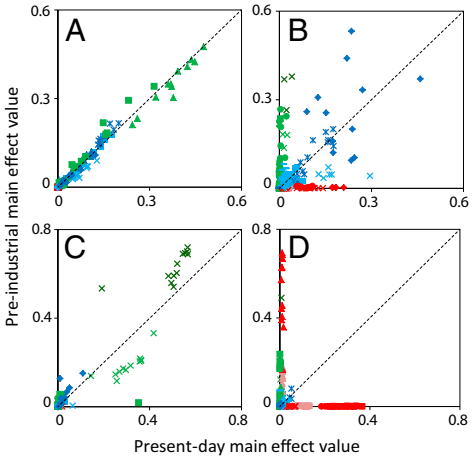

Fig. 4. The similarity of CCN sensitivities in the PI and PD to 28 parameters covering natural emissions (green), anthropogenic emissions (red), and processes (blue) for every month in the year at four different sides: (*A*) Melanesia (1°S, 151°E), (*B*) eastern Atlantic (38°N, 21°W), (*C*) Brazilian rainforest (1°S, 66°W), and (*D*) northeast China (38°N, 111°E). For more information on individual marker descriptions, please see Table S1.

suggest that fires are the largest contributor to PI CCN concentrations, major uncertainties exist as to the magnitudes of historic biomass burning emissions (20). However, in many fire-dominated regions, the response of CCN to changes in emissions is similar in both the PI and PD (e.g., Fig. 4*C*), and these regions are still likely to be useful analogs of PI CCN behavior.

Northeast China (Fig. 4*D*) has a very different CCN response and state in the two periods. Annual mean CCN concentrations at this site are the furthest from PI CCN baseline concentrations of any other location. While PI CCN concentrations are sensitive to the flux and size of biofuel emissions (from early human activity) and biogenic SOA, PD CCN concentrations are sensitive to the flux and size of fossil fuel emissions and the fraction of sulfate formed on subgrid scales from anthropogenic SO_2 emissions.

Model results spanning the grid cells 14°S to 22°S and 121°W to 130°W, which overlaps the most with the pristine region studied by Koren et al. (6) (13°S to 22°S and 121°W to 130°W), suggest that even in these remote regions PD CCN concentrations in July are up to 40% higher than in the PI. The cause of the enhanced CCN is increased biomass burning emissions. Also, the CCN response to volcanic SO_2 emissions in the region has approximately halved since the PI, and an additional PD contribution from anthropogenic SOA concentrations is seen.

The Overlap of Pristine Regions and Aerosol–Cloud Radiative Forcing. Aerosol measurements under pristine conditions would be most useful if they were made in regions where there is an aerosol–cloud radiative forcing, so that both the clean and perturbed aerosol–cloud processes could be observed. However, on average, such regions are of course not pristine today. To assess the overlap of forcing and pristine conditions, Fig. 5 shows the relationship between 1750-to-2000 monthly mean aerosol indirect radiative forcing (see *SI Methods*) and the number of pristine days per month. As expected, the general relationship shows that regions with the highest monthly mean forcing have the lowest number of pristine days (gray markers in Fig. 5). For example, grid boxes with greater than -5 Wm^{-2} forcing have generally less than five pristine days per month. When the additional constraint of similarity of CCN sensitivities is applied (tan markers in Fig. 5), it is possible to observe pristine days only in regions with a monthly mean forcing less than about -2 to -3 Wm^{-2}, which is in the lowest quartile of our forcing estimates.

If we do not restrict ourselves to observing pristine aerosol in regions of forcing, but just in regions of low cloud, then extensive

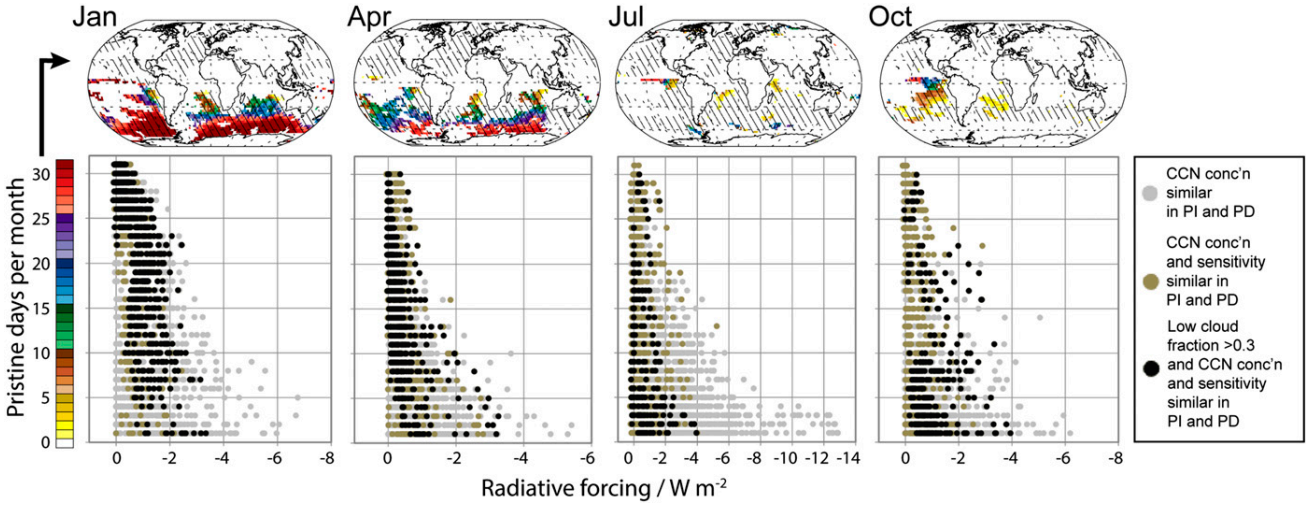

Fig. 5. The relationship between 1750-to-2000 monthly mean aerosol indirect radiative forcing and the occurrence of pristine aerosol conditions. Maps show number of days in which pristine conditions (PI:PD CCN concentrations within ±20% and similar response to the 28 parameters in both time periods) and average low cloud fraction (≥0.3; stippling) overlap.

regions can be found with pristine days of 0–31 per month. The black markers and maps in Fig. 5 show pristine regions with higher than average low cloud cover (fraction ≥0.3). These pristine low-cloud conditions generally occur over the major marine stratocumulus decks in the SH. It is in these regions where aerosol and related process measurements would be most useful in constraining the PI baseline using PD observations. However, in making aerosol–cloud measurements, there is a compromise to be reached between a useful number of observable pristine days and the magnitude of the forcing in that region. Regions with a small number of pristine days will enable strong cloud perturbations to be observed, while regions with a high number of pristine days will experience only weak or brief aerosol perturbations.

These results show that, although cloud radiative forcing and pristine regions are in general spatially anticorrelated, meteorological variability means that in regions with nonzero radiative forcing, there are days that are likely to approach PI aerosol conditions.

Conclusions

If the large uncertainty in aerosol–cloud radiative forcing between PI and PD periods is to be constrained by measurements, it is important to characterize aerosol in regions of today's atmosphere that most closely resemble PI conditions. While there is likely to always be uncertainty associated with predicting the PI atmosphere, simply because natural emissions may have changed with time, we have defined regions in today's atmosphere that are similar enough to PI conditions to be explored further. Our joint analysis of changes in CCN concentration alongside the changes in the sensitivity of CCN to emission and process perturbations provides a complete model picture of where on Earth we can observe pristine aerosol concentrations and behavior.

We have identified regions and seasons with the highest likelihood of observing pristine aerosol in terms of the number of model days per month pristine aerosol could be observed. However, ultimately, it is necessary to define pristine aerosol based on measurements because measurements are needed for model evaluation. There is no universal operational definition of pristine aerosol because natural aerosols vary substantially. The mass concentration of a species associated with anthropogenic emissions is often used as an anthropogenic tracer [e.g., carbon monoxide (19) or black carbon (40)]. However, such a definition is appropriate only if the species is not part of the local natural aerosol—clearly not the case if natural forest fire aerosols are being studied.

Our identified pristine regions may not be the only places to observe PI-like aerosol behavior. Although our model suggests that even the clean region of the Pacific studied by Koren et al. (6) has a different aerosol state and response to parameter perturbations today compared with the PI, it may still behave in a way that is sufficiently similar to the PI to be informative. However, clouds appear to be highly sensitive to aerosols at very low concentrations (3, 4, 6) and strong regime shifts can occur in some aerosol-cloud systems (8, 41), so even small perturbations of the aerosol state away from PI conditions may be important.

Our analysis has focused on daily mean regional CCN concentrations at cloud base. Precipitating shallow clouds can strongly scavenge aerosol on timescales shorter than 1 d (42, 43), leading to transient and localized conditions of very low aerosol concentration, even when the region is generally perturbed relative to the PI state by anthropogenic aerosol. The question arises whether such PD locally scavenged clean environments can be used to experimentally evaluate modeled aerosol–cloud interaction as an analog of the regional-scale response to changes in aerosols that occurred between the PI and PD. Given the different behaviors of single clouds and regional-scale cloud systems (44), it is unlikely that local processes will be informative about regional PI to PD changes that we present here. It is also important to recognize that pristine CCN environments could still be perturbed by light-absorbing aerosols either within or above the clouds (45, 46). Such effects, and associated fast adjustments of the cloud system, may alter the extent of PI-like aerosol–cloud environments shown in this study. Furthermore, pristine aerosol days may be associated with different meteorological conditions than polluted days, which would make it difficult to separate meteorological and aerosol influences on cloud behavior in PD observations.

Pristine low-cloud regions are almost entirely in the SH. To reduce the uncertainty in regions of NH forcing, we need to characterize the natural aerosol state either directly in these perturbed NH regions (which seems challenging) or in regions of the SH that are appropriate analogs for the NH. From a model uncertainty reduction perspective, an appropriate analog implies that the parameters controlling CCN sensitivity in the PI SH are the same as those controlling sensitivity in the NH. Our PI simulations of CCN suggest that CCN concentrations may have been higher in the NH than the SH, because of a larger influence of terrestrial emissions. Further research is needed to determine whether these differences limit what we can learn about NH aerosol from SH measurements.

The PI NH/SH contrast, combined with the rarity of pristine days in the NH, may mean that we have to accept that some of the

PI to PD aerosol–cloud forcing uncertainty will be irreducible. Regardless of how well we can observe and simulate aerosol–cloud interaction in today's atmosphere, a large part of the forcing uncertainty—that part associated with the unknown baseline aerosol state—will remain.

Methods

We used a global aerosol microphysics model (25), within the Toulouse Off-line Model of Chemistry and Transport (TOMCAT) (47), to simulate daily mean CCN concentrations in both the PI and the PD (see *SI Methods* for further details). Temperature fields are provided from European Centre for Medium-range Weather Forecasts, while low cloud cover is from the International Satellite Cloud Climatology Project climatology. CCN concentrations were modeled based on the median setting of 28 parameters used in Lee et al. (26), which are listed in Table S1. Emissions for both the PI and PD are listed in Table S2 and mostly follow Dentener et al. (22). Anthropogenic fossil fuel emissions are assumed to be zero in the PI, although a small anthropogenic biofuel component to the atmosphere exists (22). Natural emissions of sea spray, biogenic organic volatile compounds (which forms secondary organic aerosol), and volcanic sulfur dioxide are the same in the PI and PD. PI emissions of biofuel and biomass burning, which follow Dentener et al. (22), were derived by scaling by population, land cover, and crop production and are assigned as natural aerosol, although, in reality, these emissions could be a result of both anthropogenic (land/agricultural clearance) and natural (wildfire) activity. The model has previously been extensively evaluated against observations (see *SI Methods*), and model–observation bias is low in both clean and polluted regions (28). A variance-based sensitivity analysis of PI CCN concentrations to perturbations of the 28 model parameters covering emissions, microphysics, and model structures was performed in the same way as the PD analysis of Lee et al. (26) (see *SI Methods*). The 28 model parameters and their ranges are defined in Table S1, with a full description of what each parameter does in the model in Lee et al. (26). Parameters relating to biomass burning emissions are assigned as natural aerosol in both PI and PD. Accurate source type identification of biomass burning aerosol with similar fuel type is currently impossible to disentangle in the atmosphere once the aerosol becomes well mixed. In combination with the similar assumption of PI BB emissions, we therefore expect that our identification of pristine aerosol in fire-dominated environments will be an upper limit. The modeled CCN concentrations and the sensitivity analysis used 2008 meteorology in each modeled time period. We define CCN concentrations as the aerosol concentration with a dry diameter above 50 nm that are reported at 915 hPa, typical of cloud base for stratiform low-level clouds. An analysis of the vertical profile of pristine regions (see *SI Methods*) shows little variation within the boundary layer. Radiative forcing values reported in Carslaw et al. (4), which were derived from the same set of PI and PD experiments, were also used in this study.

ACKNOWLEDGMENTS. D.S.H. would like to thank Masaru Yoshioka for additional data relating to Figs. S7 and S8, Graham Mann and Gerd Folberth for their comments, and the Natural Environment Research Council and Met Office for funding his Ph.D. This research has received funding from the Natural Environment Research Council Aerosol Robustness and Sensitivity Project (NE/G006172/1) and Global Aerosol Synthesis and Science Project Project (NE/J024252/1), National Centre for Atmospheric Science, as well as the European Union BACCHUS project under Grant Agreement 603445. K.S.C. is currently a Royal Society Wolfson Merit Award holder.

1. Carslaw KS, et al. (2010) A review of natural aerosol interactions and feedbacks within the Earth system. *Atmos Chem Phys* 10(4):1701–1737.
2. Rap A, et al. (2013) Natural aerosol direct and indirect radiative effects. *Geophys Res Lett* 40(12):3297–3301.
3. Schmidt A, et al. (2012) Importance of tropospheric volcanic aerosol for indirect radiative forcing of climate. *Atmos Chem Phys* 12(16):7321–7339.
4. Carslaw KS, et al. (2013) Large contribution of natural aerosols to uncertainty in indirect forcing. *Nature* 503(7474):67–71.
5. Jones A, Roberts DL, Slingo A (1994) A climate model study of indirect radiative forcing by anthropogenic sulphate aerosols. *Nature* 370:450–453.
6. Koren I, Dagan G, Altaratz O (2014) From aerosol-limited to invigoration of warm convective clouds. *Science* 344(6188):1143–1146.
7. Menon S, Genio ADD, Koch D, Tselioudis G (2002) GCM simulations of the aerosol indirect effect: Sensitivity to cloud parameterization and aerosol burden. *J Atmos Sci* 59:692–713.
8. Rosenfeld D, Sherwood S, Wood R, Donner L (2014) Atmospheric science. Climate effects of aerosol-cloud interactions. *Science* 343(6169):379–380.
9. Otto A, et al. (2013) Energy budget constraints on climate response. *Nat Geosci* 6:415–416.
10. Mahowald N (2011) Aerosol indirect effect on biogeochemical cycles and climate. *Science* 334(6057):794–796.
11. Penner JE, Zhou C, Xu L (2012) Consistent estimates from satellites and models for the first aerosol indirect forcing. *Geophys Res Lett* 39(13):L13810.
12. Andreae MO (2007) Atmosphere. Aerosols before pollution. *Science* 315(5808):50–51.
13. Manktelow PT, Carslaw KS, Mann GW, Spracklen DV (2009) Variable CCN formation potential of regional sulfur emissions. *Atmos Chem Phys* 9:3253–3259.
14. Tunved P, et al. (2006) High natural aerosol loading over boreal forests. *Science* 312(5771):261–263.
15. Martin ST, et al. (2010) An overview of the Amazonian Aerosol Characterization Experiment 2008 (AMAZE-08). *Atmos Chem Phys* 10(23):11415–11438.
16. Pöschl U, et al. (2010) Rainforest aerosols as biogenic nuclei of clouds and precipitation in the Amazon. *Science* 329(5998):1513–1516.
17. Murphy DM, et al. (1998) Influence of sea-salt on aerosol radiative properties in the Southern Ocean marine boundary layer. *Nature* 392:62–65.
18. Fiebig M, et al. (2014) Annual cycle of Antarctic baseline aerosol: Controlled by photooxidation-limited aerosol formation. *Atmos Chem Phys* 14(6):3083–3093.
19. Clarke A, Kapustin V (2010) Hemispheric aerosol vertical profiles: Anthropogenic impacts on optical depth and cloud nuclei. *Science* 329(5998):1488–1492.
20. Marlon JR, et al. (2008) Climate and human influences on global biomass burning over the past two millennia. *Nat Geosci* 1:697–702.
21. Riccobono F, et al. (2014) Oxidation products of biogenic emissions contribute to nucleation of atmospheric particles. *Science* 344(6185):717–721.
22. Dentener F, et al. (2006) Emissions of primary aerosol and precursor gases in the years 2000 and 1750 prescribed data-sets for AeroCom. *Atmos Chem Phys* 6:4321–4344.
23. Schulz M, et al. (2006) Radiative forcing by aerosols as derived from the AeroCom present-day and pre-industrial simulations. *Atmos Chem Phys* 6:5225–5246.
24. Andreae MO, Rosenfeld D (2008) Aerosol–cloud–precipitation interactions. Part 1. The nature and sources of cloud-active aerosols. *Earth Sci Rev* 89(1-2):13–41.
25. Mann GW, et al. (2010) Description and evaluation of GLOMAP-mode: A modal global aerosol microphysics model for the UKCA composition-climate model. *Geosci Model Dev* 3(2):519–551.
26. Lee LA, et al. (2013) The magnitude and causes of uncertainty in global model simulations of cloud condensation nuclei. *Atmos Chem Phys* 13(17):8879–8914.
27. Merikanto J, Spracklen DV, Mann GW, Pickering SJ, Carslaw KS (2009) Impact of nucleation on global CCN. *Atmos Chem Phys* 9:8601–8616.
28. Spracklen DV, Carslaw KS, Pöschl U, Rap A, Forster PM (2011) Global cloud condensation nuclei influenced by carbonaceous combustion aerosol. *Atmos Chem Phys* 11(17):9067–9087.
29. Capaldo K, Corbett J, Kasibhatla P, Fischbeck P, Pandis SN (1999) Effects of ship emissions on sulphur cycling and radiative climate forcing over the ocean. *Nature* 400:743–746.
30. Korhonen H, Carslaw KS, Spracklen DV, Mann GW, Woodhouse MT (2008) Influence of oceanic dimethyl sulfide emissions on cloud condensation nuclei concentrations and seasonality over the remote Southern Hemisphere oceans: A global model study. *J Geophys Res* 113:D15204.
31. Bowman DMJS, et al. (2009) Fire in the Earth system. *Science* 324(5926):481–484.
32. Pierce JR, et al. (2012) Nucleation and condensational growth to CCN sizes during a sustained pristine biogenic SOA event in a forested mountain valley. *Atmos Chem Phys* 12(7):3147–3163.
33. Chi X, et al. (2013) Long-term measurements of aerosol and carbon monoxide at the ZOTTO tall tower to characterize polluted and pristine air in the Siberian taiga. *Atmos Chem Phys* 13(24):12271–12298.
34. Browse J, Carslaw KS, Arnold SR, Pringle K, Boucher O (2012) The scavenging processes controlling the seasonal cycle in Arctic sulphate and black carbon aerosol. *Atmos Chem Phys* 12(15):6775–6798.
35. Bond TC, et al. (2013) Bounding the role of black carbon in the climate system: A scientific assessment. *J Geophys Res* 118(11):5380–5552.
36. Yu H, et al. (2012) Aerosols from overseas rival domestic emissions over North America. *Science* 337(6094):566–569.
37. Lee LA, Carslaw KS, Pringle KJ, Mann GW (2012) Mapping the uncertainty in global CCN using emulation. *Atmos Chem Phys* 12(20):9739–9751.
38. Savoie DL, Prospero JM, Merrill JT, Uematsu M (1989) Nitrate in the atmospheric boundary layer of the tropical South Pacific: Implications regarding sources and transport. *J Atmos Chem* 8:391–415.
39. Spracklen DV, Rap A (2013) Natural aerosol-climate feedbacks suppressed by anthropogenic aerosol. *Geophys Res Lett* 40(19):5316–5319.
40. O'Dowd CD, et al. (2004) Biogenically driven organic contribution to marine aerosol. *Nature* 431(7009):676–680.
41. Mechoso CR, et al. (2014) Ocean–Cloud–Atmosphere–Land Interactions in the Southeastern Pacific: The VOCALS Program. *Bull Am Meteorol Soc* 95(3):357–375.
42. Muhlbauer A, McCoy IL, Wood R (2014) Climatology of stratocumulus cloud morphologies: microphysical properties and radiative effects. *Atmos Chem Phys* 14(13):6695–6716.
43. Wood R, et al. (2008) Open cellular structure in marine stratocumulus sheets. *J Geophys Res* 113(D12):1–16.
44. Stevens B, Feingold G (2009) Untangling aerosol effects on clouds and precipitation in a buffered system. *Nature* 461(7264):607–613.
45. Ackerman AS, et al. (2000) Reduction of tropical cloudiness by soot. *Science* 288(5468):1042–1047.
46. Wilcox EM (2010) Stratocumulus cloud thickening beneath layers of absorbing smoke aerosol. *Atmos Chem Phys* 10(23):11769–11777.
47. Chipperfield MP (2006) New version of the TOMCAT/SLIMCAT off-line chemical transport model: Intercomparison of stratospheric tracer experiments. *Q J R Meteorol Soc* 132(617):1179–1203.

Supporting Information

Hamilton et al. 10.1073/pnas.1415440111

SI Methods

Model Description. The Global Modal of Aerosol Processes (GLOMAP-mode) is a size-resolving global 3D aerosol microphysics model (1) within the TOMCAT chemistry transport model (2). GLOMAP-mode generates aerosol size and number distribution in seven lognormal modes (one soluble nucleation mode, plus one insoluble and one soluble for each of the Aitken, accumulation, and coarse modes). To speed up computation of the model ensemble, 3D gas-phase chemical fields were generated from a single global chemistry simulation of TOMCAT. These fields provide oxidant concentrations (ozone as well as OH and NO_3 radicals) at 3-hourly intervals, which are used in GLOMAP to calculate the oxidation of aerosol precursor gases.

GLOMAP-mode has previously been used to simulate cloud condensation nuclei (CCN) concentrations in various studies involving natural aerosol (3–6) and has been shown to perform well against a compilation of global CCN measurements in different environments (7). In addition, the model has been evaluated against extensive aerosol observations (1) and refined by comparing against a more detailed bin-resolved version of the model (8). GLOMAP has been widely evaluated against global measurements of particle number concentrations (9, 10), aerosol chemical components (7, 11, 12), and cloud droplets (13). Vertical profiles of aerosol number concentrations in GLOMAP have been compared with other similar models, and performance is comparable (14).

The perturbed parameter GLOMAP ensemble [previously reported (15, 16)] and the single-hourly output simulations for 1750 and 2000 were set up in an identical way. The 28 perturbed parameters were set to the median value of the single runs (Table S1), where the total uncertainty distributions are represented by beta distributions. All model runs used an effective grid horizontal resolution of 2.8° × 2.8° with 31 vertical levels between the surface and 10 hPa. Unless otherwise stated, all CCN concentrations are reported at 915 hPa (approx. 850 m a.s.l.) to be relevant for cloud base. All simulations used meteorology for the year 2008 from European Centre for Medium-range Weather Forecasts reanalyses.

Global annual emission fluxes used in the single-hourly output simulations are listed in Table S2. The model includes a dust scheme and is simulated in this study; however, as dust has shown dust to have little effect on CCN concentrations, even in dust storms (17), we do not evaluate the individual impact of dust on CCN concentrations.

Sensitivity Analysis and CCN Uncertainty Estimation. An emulator of PI monthly mean CCN concentration was built for each grid cell of the model on the 915-hPa model level. The Bayesian emulator (18) describes the relationship between the modeled CCN and the setting of the 28 perturbed parameters across the defined uncertainty space in Table S1. As in Lee et al. (16), an emulator training set of 168 global annual model simulations was used, with combinations of parameter settings defined by a maximum Latin Hypercube experimental design. A further 84 emulator validation runs were also performed.

Here we studied the monthly main effect values to evaluate the sensitivity of CCN to each of the 28 parameters, having shown in Lee et al. (16) that interactions between parameters contribute a small fraction of overall CCN variance. The main effect is therefore the fraction of the variance associated with the perturbation of that parameter only, and is equal to the fraction of the variance that would be removed if that parameter were known exactly. The main effect values were calculated using variance decomposition of 140,000 Monte Carlo CCN samples drawn from the emulator.

To estimate the uncertainty in PI CCN in each grid cell, the SD around the monthly mean PI CCN concentrations was calculated as the square root of the total variance due to uncertainty in the 28 parameters and their interactions (16). As stated in the *Results and Discussion, Properties of the Preindustrial Aerosol*, this approach generates a probability density distribution of CCN concentrations caused by the uncertainty in the model input parameters, including their interactions.

To identify grid cells with similar CCN sensitivity in the PI and PD, the goodness of fit correlation (coefficient of determination) of the 28 PI and PD parameter sensitivities (main effects) was calculated. The goodness of fit is based on the 1:1 line by setting the predicted value in the residual sum of squares calculation equal to the observed value (i.e., the expected PD main effect = the initial PI main effect) and not on the best fit line. We then consider those grid cells that have an $r^2 \geq 0.9$ as having a pristine "PI-like" sensitivity (i.e., the CCN sensitivity to all 28 parameters is behaving similarly in both time periods). Although it is possible for the CCN response to a single parameter to be of an equal and opposite sign of magnitude, this is unlikely and does not alter the concept that the sensitivity of the aerosol to the full 28-parameter ensemble is still similar.

Radiative Forcing Calculations. Radiative forcing values were obtained from the Carslaw et al. (15) study and compared with pristine regions identified in this study. The forcing is calculated as the difference at the top-of-the atmosphere net short-wave plus long-wave radiative fluxes between the PI and PD time periods using the offline Edwards and Slingo radiative transfer model (19). Cloud drop number concentrations are calculated in both the PI and PD, from which the magnitude of the forcing is calculated. Forcing estimates were then linearly interpolated onto the 2.8° by 2.8° GLOMAP grid to allow direct comparison with both the simulation and emulation results. Low-cloud fraction is taken from a climatology of observations created by the International Satellite Cloud Climatology Project (ISCCP-D2) (20) and again were linearly interpolated onto the GLOMAP grid.

1. Mann GW, et al. (2010) Description and evaluation of GLOMAP-mode: A modal global aerosol microphysics model for the UKCA composition-climate model. *Geosci Model Dev* 3:519–551.
2. Chipperfield MP (2006) New version of the TOMCAT/SLIMCAT off-line chemical transport model: Intercomparison of stratospheric tracer experiments. *Q J R Meteorol Soc* 132:1179–1203.
3. Schmidt A, et al. (2010) The impact of the 1783–1784 AD Laki eruption on global aerosol formation processes and cloud condensation nuclei. *Atmos Chem Phys* 10:6025–6041.
4. Woodhouse MT, et al. (2010) Low sensitivity of cloud condensation nuclei to changes in the sea-air flux of dimethyl-sulphide. *Atmos Chem Phys* 10:7545–7559.
5. Spracklen DV, Rap A (2013) Natural aerosol-climate feedbacks suppressed by anthropogenic aerosol. *Geophys Res Lett* 40(19):5316–5319.
6. Scott CE, et al. (2014) The direct and indirect radiative effects of biogenic secondary organic aerosol. *Atmos Chem Phys* 14:447–470.
7. Spracklen DV, Carslaw KS, Pöschl U, Rap A, Forster PM (2011) Global cloud condensation nuclei influenced by carbonaceous combustion aerosol. *Atmos Chem Phys* 11:9067–9087.
8. Mann GW, et al. (2012) Intercomparison of modal and sectional aerosol microphysics representations within the same 3-D global chemical transport model. *Atmos Chem Phys* 12:4449–4476.
9. Spracklen DV, et al. (2010) Explaining global surface aerosol number concentrations in terms of primary emissions and particle formation. *Atmos Chem Phys* 10:4775–4793.
10. Reddington CL, et al. (2011) Primary versus secondary contributions to particle number concentrations in the European boundary layer. *Atmos Chem Phys* 11:12007–12036.

11. Browse J, Carslaw KS, Arnold SR, Pringle K, Boucher O (2012) The scavenging processes controlling the seasonal cycle in Arctic sulphate and black carbon aerosol. *Atmos Chem Phys* 12:6775–6798.
12. Schmidt A, et al. (2011) Excess mortality in Europe following a future Laki-style Icelandic eruption. *Proc Natl Acad Sci USA* 108(38):15710–15715.
13. Pringle KJ, et al. (2012) A multi-model assessment of the impact of sea spray geoengineering on cloud droplet number. *Atmos Chem Phys* 12:11647–11663.
14. Mann GW, et al. (2014) Intercomparison and evaluation of global aerosol microphysical properties among AeroCom models of a range of complexity. *Atmos Chem Phys* 14:4679–4713.
15. Carslaw KS, et al. (2013) Large contribution of natural aerosols to uncertainty in indirect forcing. *Nature* 503(7474):67–71.
16. Lee LA, et al. (2013) The magnitude and causes of uncertainty in global model simulations of cloud condensation nuclei. *Atmos Chem Phys* 13:8879–8914.
17. Manktelow PT, Carslaw KS, Mann GW, Spracklen DV (2010) The impact of dust on sulfate aerosol, CN and CCN during an East Asian dust storm. *Atmos Chem Phys* 10: 365–382.
18. Lee L, Carslaw K, Pringle K, Mann G, Spracklen D (2011) Emulation of a complex global aerosol model to quantify sensitivity to uncertain parameters. *Atmos Chem Phys* 11:12253–12273.
19. Edwards J, Slingo A (1996) Studies with a flexible new radiation code. I: Choosing a configuration for a large scale model. *Q J R Meteorol Soc* 122:689–719.
20. Rossow WB, Schiffer RA (1999) Advances in understanding clouds from ISCCP. *Bull Am Meteorol Soc* 80:2261–2287.

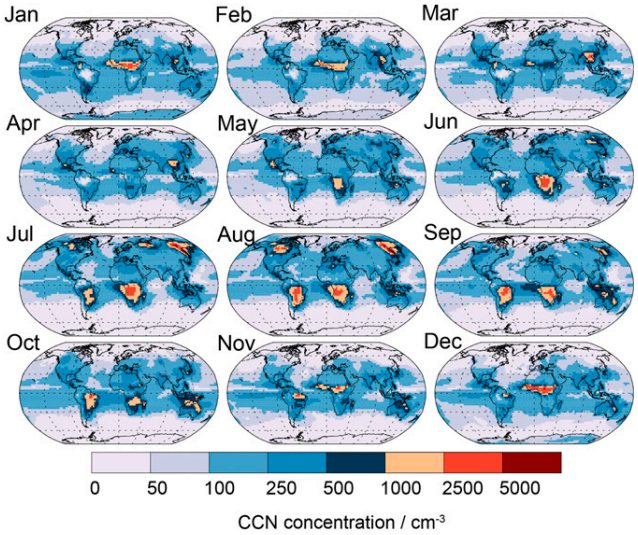

Fig. S1. PI (1750) CCN concentrations. Monthly mean concentrations were calculated from daily mean modeled CCN concentrations at cloud base (~915 hPa).

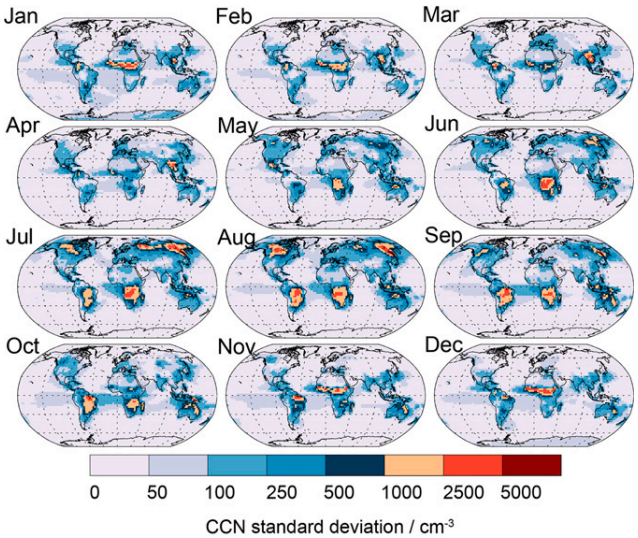

Fig. S2. PI (1750) CCN concentration SD at 915 hPa.

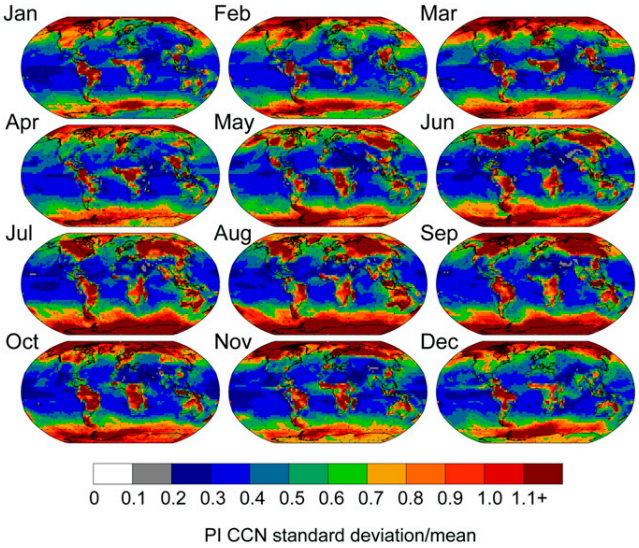

Fig. S3. PI (1750) CCN relative SD (SD/mean) at 915 hPa.

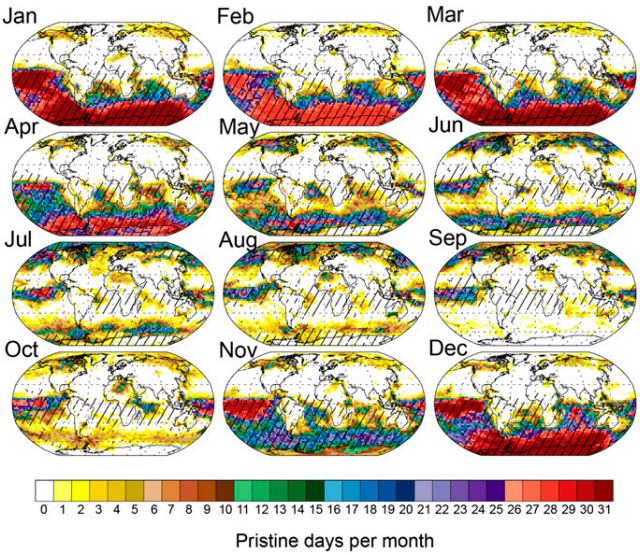

Fig. S4. The occurrence of pristine days over 1 y, based on two definitions. Colors show the number of days per month on which PI and PD CCN concentrations differ by no more than ±20% in that grid cell at cloud base (~915 hPa). Stippling shows regions where the sensitivities of PI and PD CCN to 28 model parameters are similar ($r^2 \geq 0.9$) in that grid cell at cloud base.

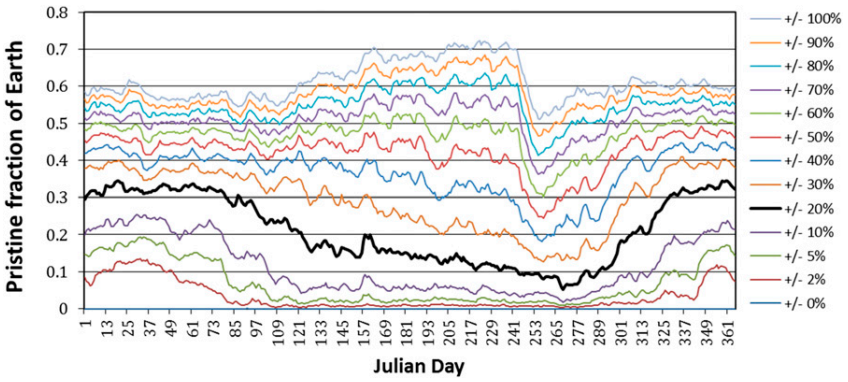

Fig. S5. The fraction of the Earth defined as pristine based on the PI to PD CCN concentration change being within a certain threshold. Thresholds vary from ±0% to ±100%. Results are for every day over a full year with CCN concentrations taken at 915 hPa in every grid cell of the model.

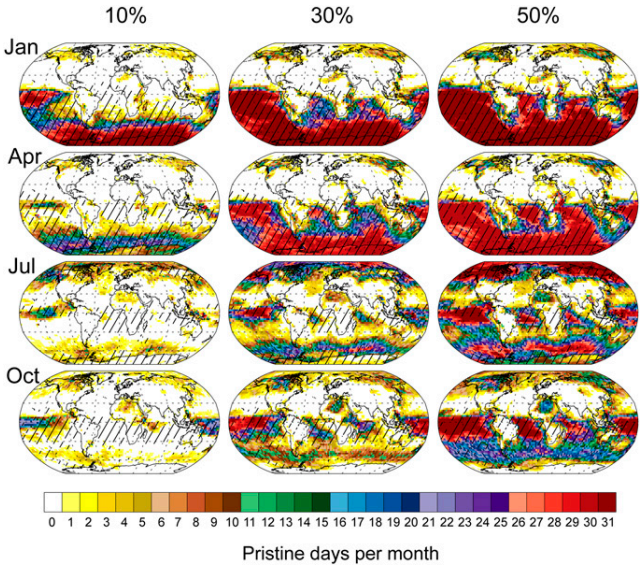

Fig. S6. The occurrence of pristine days in January, April, July, and October based on two definitions. Colors show the number of days per month on which PI and PD CCN concentrations differ by either ±10%, ±30%, or ±50% in that grid cell at cloud base (~915 hPa). Stippling shows regions where the sensitivities of PI and PD CCN to 28 model parameters are similar ($r^2 \geq 0.9$) in that grid cell at cloud base.

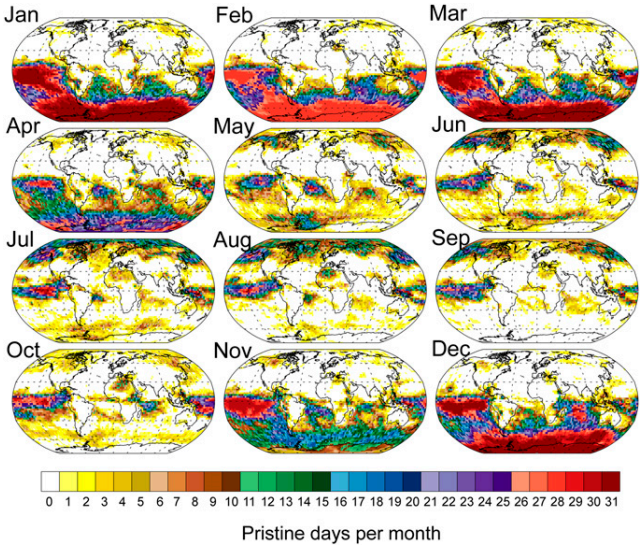

Fig. S7. The occurrence of pristine days over 1 y. Colors show the number of days per month on which PI and PD CCN concentrations differ by no more than ±20% in that grid cell at ~2500 m.

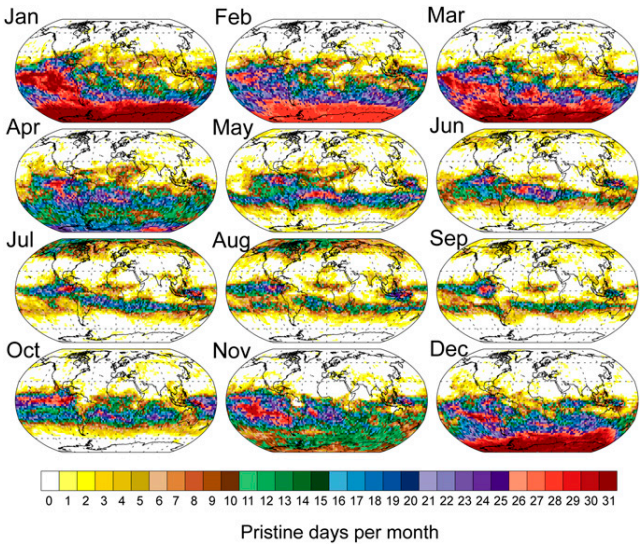

Fig. S8. The occurrence of pristine days over 1 y. Colors show the number of days per month on which PI and PD CCN concentrations differ by no more than ±20% in that grid cell at ~5,000 m.

Table S1. Parameter descriptions, uncertainty ranges and median values as used in both the PI and PD model runs

Parameter description	Uncertainty range	Median value	Effect	Symbol (Fig. 4)
Volcanic SO_2 emission flux	0.5–2	1	scaled	▲
Biogenic monoterpene production of secondary organic aerosol	5–360 Tg POM per year*	50 Tg POM per year*	absolute	■
Sea spray mass flux (coarse/accumulation)	0.2–5	1	scaled	●
DMS emission flux	0.5–2	1	scaled	◆
Biomass burning mass emission rate (BC/OC)	0.25–4	1	scaled	✖
Biomass burning emitted median dry diameter (BC/OC)	50–200 nm	110 nm	absolute	✖
Fossil fuel mass emission rate (BC/OC)	0.5–2	1	scaled	■
Fossil fuel emitted median dry diameter (BC/OC)	30–80 nm	56 nm	absolute	■
Biofuel mass emission rate (BC/OC)	0.25–4	1	scaled	▲
Biofuel emitted median dry diameter (BC/OC)	50–200 nm	110 nm	absolute	▲
Mass fraction of SO_2 converted to new sulfate particles in subgrid power plant plumes	0–1%	0.0012%	scaled	●
Emitted number median dry diameter of new subgrid sulfate particles	20–100 nm	40 nm	absolute	●
Anthropogenic SO_2 emission flux	0.6–1.5	1	scaled	✖
Anthropogenic VOC production of secondary organic aerosol	2–112 Tg POM per year*	80 Tg POM per year*	absolute	◆
Boundary layer nucleation rate coefficient	$3.2x10^{-7}$-2 x 10^{-4} s^{-1}	2.6 x 10^{-7} s^{-1}	absolute	■
Free tropospheric nucleation rate	0.01–10	1	scaled	■
Aging	0.3–5 monolayer	1 monolayer	absolute	●
Accumulation modal width (soluble/insoluble)	1.2–1.8	1.5	scaled	✖
Aitken modal width (soluble/insoluble)	1.2–1.8	1.5	scaled	✖
Mode separation diameter (nucleation/Aitken)	9–18 nm	10 nm	absolute	✚
Mode separation diameter (Aitken/accumulation)	0.9–2 x activation diameter	1.5	scaled	✚
Cloud drop activation dry diameter	50–100 nm	75 nm	absolute	▲
pH of cloud drops (controls SO_2 + O_3)	pH 4–6.5	pH 5.5	absolute	✖
pH of cloud drops (SO_2 + O_3)	pH 3.5–5	pH 4	absolute	✖
Nucleation scavenging offset dry diameter	0–50 nm	25 nm	absolute	–
Nucleation scavenging fraction (accumulation mode) in mixed and ice clouds (T < –15C)	0–1	0.5	scaled	–
Dry deposition velocity of Aitken mode	0.5–2	1	scaled	◆
Dry deposition velocity of accumulation mode	0.1–10	1	scaled	◆

For the emissions, the median value of the scaling parameter means that the emissions in Table S2 were used. Symbols relate to those seen in Fig. 4.

Table S2. Emissions of aerosols and precursor gases used in the simulations

Source	Emitted species	PD (2000) flux	PI (1750) flux	Reference
Fossil fuel	BC	3.0 $Tg{\cdot}a^{-1}$ C	zero	(1)
	POM	3.2 $Tg{\cdot}a^{-1}$ POM	zero	(1)
Power stations	SO_2	24.2 $Tg{\cdot}a^{-1}$ S	zero	(1, 2)
Industrial processes	SO_2	19.6 $Tg{\cdot}a^{-1}$ S	zero	(1, 2)
Transportation	SO_2	4.8 $Tg{\cdot}a^{-1}$ S	zero	(1, 2)
Off-road	SO_2	0.8 $Tg{\cdot}a^{-1}$ S	zero	(1, 2)
Biofuel	BC	1.6 $Tg{\cdot}a^{-1}$ C	0.4 $Tg{\cdot}a^{-1}$ C	(1, 3)
	POM	9.1 $Tg{\cdot}a^{-1}$ POM	1.6 $Tg{\cdot}a^{-1}$ POM	(1, 3)
Domestic	SO_2	4.8 $Tg{\cdot}a^{-1}$ S	0.12 $Tg{\cdot}a^{-1}$ S	(1, 3)
Wildfires	BC	3.1 $Tg{\cdot}a^{-1}$ C	1.03 $Tg{\cdot}a^{-1}$ C	(1, 4)
	POM	34.7 $Tg{\cdot}a^{-1}$ POM	12.8 $Tg{\cdot}a^{-1}$ POM	(1, 4)
	SO_2	2.1 $Tg{\cdot}a^{-1}$ S	1.46 $Tg{\cdot}a^{-1}$ S	(1, 4)
Volcanoes	SO_2	12.6 $Tg{\cdot}a^{-1}$ S	12.6 $Tg{\cdot}a^{-1}$ S	(5)
Marine dimethyl sulphide	DMS[a]	17.1 $Tg{\cdot}a^{-1}$ S	17.1 $Tg{\cdot}a^{-1}$ S	(6)
Sea spray	salt	wind-dependent flux	same as PD	(7)
Biogenic volatile organic carbon	Monoterpenes (α-pinene)	50 $Tg{\cdot}a^{-1}$ POM produced	50 $Tg{\cdot}a^{-1}$ POM produced	(8, 9) (for spatial/temporal variation)
Anthropogenic volatile organic carbon	VOC	80 $Tg{\cdot}a^{-1}$ POM produced	zero	(8)

[a]The DMS emission flux is a global annual value but emissions are calculated at each timestep based on the seawater DMS concentration field (6) and a sea-air transfer velocity (10).

1. Dentener F, et al. (2006) The global atmospheric environment for the next generation. *Environ Sci Technol* 40(11):3586–3594.
2. Cofala J, Amann M, Mechler R (2005) Scenarios of world anthropogenic emissions of air pollutants and methane up to 2030 (Int Inst Appl Syst Res, Laxenburg, Austria), Interim Rep IR-06-023.
3. Bond TC, et al. (2013) Bounding the role of black carbon in the climate system: A scientific assessment. *J Geophys Res* 118(11):5380–5552.
4. Van Der Werf GR, Randerson JT, Collatz GJ, Giglio L (2003) Carbon emissions from fires in tropical and subtropical ecosystems. *Glob Change Biol* 9:547–562.
5. Andres RJ, Kasgnoc AD (1998) A time-averaged inventory of subaerial volcanic. *J Geophys Res* 103:25,251–25,261.
6. Kettle A, Andreae M (2000) Flux of dimethylsulfide from the oceans: A comparison of updated data sets and flux models. *J Geophys Res* 105:26,793–26,808.
7. Ayash T, Gong S, Jia CQ (2008) Direct and indirect shortwave radiative effects of sea salt aerosols. *J Clim* 21:3207–3220.
8. Spracklen DV, et al. (2011) Aerosol mass spectrometer constraint on the global secondary organic aerosol budget. *Atmos Chem Phys* 11:12109–12136.
9. Guenther A, et al. (1995) A global model of natural volatile organic compound emissions. *J Geophys Res* 100:8873–8892.
10. Nightingale PD, Liss PS, Schlosser P (2000) Measurements of air-sea gas transfer during an open ocean algal bloom. *Geophys Res Lett* 27:2117–2120.